The Astrophysical Journal, 693:1610–1620, 2009 March 10 doi:10.1088/0004-637X/693/2/1610

GRB 080913 AT REDSHIFT 6.7

J. Greiner[1], T. Krühler[1,2], J. P. U. Fynbo[3], A. Rossi[4], R. Schwarz[5], S. Klose[4], S. Savaglio[1], N. R. Tanvir[6], S. McBreen[1], T. Totani[7], B. B. Zhang[8], X. F. Wu[9,10], D. Watson[3], S. D. Barthelmy[11], A. P. Beardmore[6], P. Ferrero[4], N. Gehrels[11], D. A. Kann[4], N. Kawai[12], A. Küpcü Yoldaş[13], P. Mészáros[9,14], B. Milvang-Jensen[3], S. R. Oates[15], D. Pierini[1], P. Schady[15], K. Toma[9,16], P. M. Vreeswijk[3], A. Yoldaş[1], B. Zhang[8], P. Afonso[1], K. Aoki[17], D. N. Burrows[9], C. Clemens[1], R. Filgas[1], Z. Haiman[18], D. H. Hartmann[19], G. Hasinger[1], J. Hjorth[3], E. Jehin[20], A. J. Levan[21], E. W. Liang[22], D. Malesani[3], T.-S. Pyo[17], S. Schulze[4], G. Szokoly[1,23], and K. Terada and K. Wiersema[6]

[1] Max-Planck-Institut für extraterrestrische Physik, Giessenbachstraße 1, D-85740 Garching, Germany
[2] Universe Cluster, Technische Universität München, Boltzmannstraße 2, D-85748, Garching, Germany
[3] Dark Cosmology Centre, Niels Bohr Institute, University of Copenhagen, Juliane Maries Vej 30, DK-2100 København Ø, Denmark
[4] Thüringer Landessternwarte Tautenburg, Sternwarte 5, D-07778 Tautenburg, Germany
[5] Astrophysical Institute Potsdam, D-14482 Potsdam, An der Sternwarte 16, Germany
[6] Department of Physics and Astronomy, University of Leicester, University Road, Leicester LE1 7RH, UK
[7] Department of Astronomy, Kyoto University, Sakyo-ku, Kyoto 606-8502, Japan
[8] Department of Physics and Astronomy, University of Nevada, 4505 Maryland Parkway, Las Vegas, NV 89154-4002, USA
[9] Department of Astronomy & Astrophysics, Pennsylvania State University, 525 Davey Lab, University Park, PA 16802, USA
[10] Purple Mountain Observatory, Chinese Academy of Sciences, Nanjing 210008, China
[11] NASA-GSFC, Code 661, Greenbelt, MD 20771, USA
[12] Department of Physics, Tokyo Inst. of Technology, 2-12-1 Ookayama, Meguro-ku, Tokyo 152-8551, Japan
[13] ESO, Karl-Schwarzschild-Str. 2, 85740 Garching, Germany
[14] Department of Physics, Pennsylvania State University, 525 Davey Lab, University Park, PA 16802, USA
[15] Mullard Space Science Lab, University College London, Holmbury St. Mary, Dorking, Surrey, RH5 6NT, UK
[16] Division of Theoretical Astronomy, National Astronomical Observatory of Japan, 2-21-1 Osawa, Mitaka, Tokyo 181-8588, Japan
[17] Subaru Telescope, National Astronomical Observatory of Japan, 650 North A'ohōkū Place, Hilo, HI 96720, USA
[18] Department of Astronomy, Columbia University, 1328 Pupin Physics Laboratories, New York, NY 10027, USA
[19] Department of Physics and Astronomy, Clemson University, Clemson, SC 29634, USA
[20] Inst. d'Astrophysique de l'Université de Liège, Allée du 6 Août 17, B-4000 Liège, Belgium
[21] Department of Physics, University of Warwick, Coventry CV4 7AL, UK
[22] Department of Physics, Guangxi University, Guangxi 53004, China
[23] Eötvös Univ., 1117 Budapest, Pazmany P. stny. 1/A, Hungary
Received 2008 October 13; accepted 2008 December 4; published 2009 March 10

ABSTRACT

We report on the detection by *Swift* of GRB 080913, and subsequent optical/near-infrared follow-up observations by GROND, which led to the discovery of its optical/NIR afterglow and the recognition of its high-z nature via the detection of a spectral break between the i' and z' bands. Spectroscopy obtained at the ESO-VLT revealed a continuum extending down to $\lambda = 9400$ Å, and zero flux for 7500 Å$< \lambda <$ 9400 Å, which we interpret as the onset of a Gunn–Peterson trough at $z = 6.695 \pm 0.025$ (95.5% confidence level), making GRB 080913 the highest-redshift gamma-ray burst (GRB) to date, and more distant than the highest-redshift QSO. We note that many redshift indicators that are based on promptly available burst or afterglow properties have failed for GRB 080913. We report on our follow-up campaign and compare the properties of GRB 080913 with bursts at lower redshift. In particular, since the afterglow of this burst is fainter than typical for GRBs, we show that 2 m class telescopes can identify most high-redshift GRBs.

Key words: early universe – gamma rays: bursts – radiation mechanisms: non-thermal

Online-only material: color figures

1. INTRODUCTION

The potential of gamma-ray bursts (GRBs) as beacons to the distant universe has long been recognized. The immense luminosity of both the prompt gamma-ray emission and X-ray and optical afterglows indicates that GRBs should, with present-day technology such as *Swift*/BAT, be visible out to distances of $z > 10$ (Lamb & Reichart 2000; Gou et al. 2004). Due to their connection to the death of massive stars (Woosley 1993; Galama et al. 1998; Hjorth et al. 2003; Stanek et al. 2003), long GRBs probe the evolution of cosmic star formation (Totani 1997; Wijers et al. 1998; Chary et al. 2007; Yüksel et al. 2008), reionization of the intergalactic medium (Miralda-Escude 1998; Totani et al. 2006), and the metal enrichment history of the universe (e.g., Hartmann et al. 2004; Fynbo et al. 2006; Savaglio 2006; Berger et al. 2006; Prochaska et al. 2007). Despite this potential and the high detection rate now delivered by *Swift*, finding bursts out to the highest redshifts has proved a challenging task. The hitherto highest redshift burst, GRB 050904 at $z = 6.29$ (Tagliaferri et al. 2005; Kawai et al. 2006; Haislip et al. 2006), held the record for three years and in that time only GRB 060927 at $z = 5.47$ (Ruiz-Velasco et al. 2007) came close.

In part, this owes much to the intrinsic difficulty in locating such bursts. At $z > 5.5$ afterglows become essentially invisible to observers in the R band, where much follow-up is attempted. Often the mere time required to obtain a photometric selection of high-z candidates is so long that the afterglow is too faint for spectroscopic follow-up. Furthermore, although the campaigns on GRB 050904 were extremely successful, this burst was far from a typical event. Indeed, its peak optical luminosity rivaled

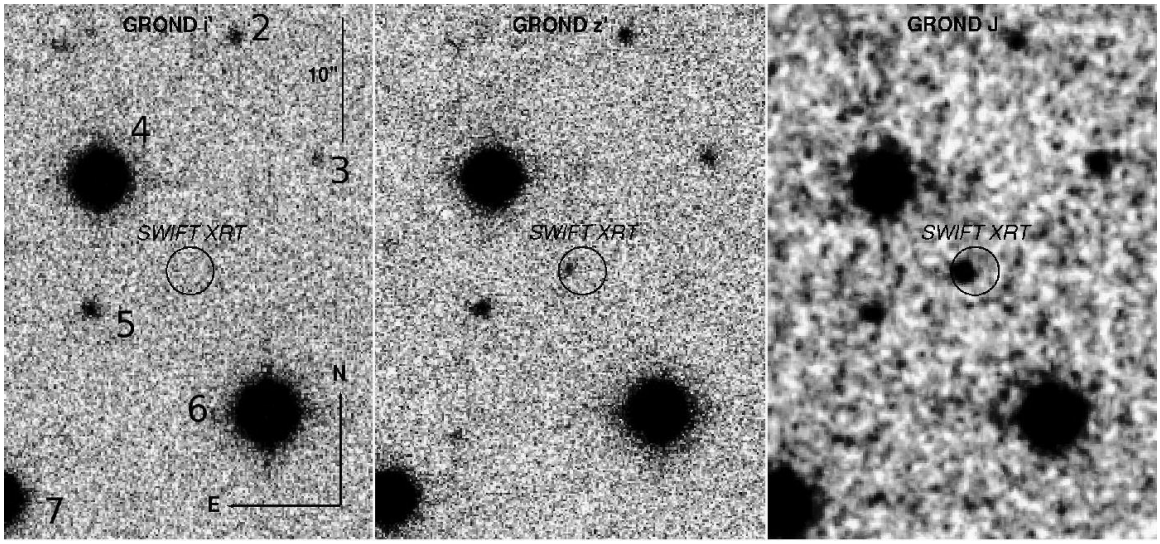

Figure 1. i'- (left), z'- (middle), and J- (right) band images of the afterglow of GRB 080913 obtained with the seven-channel imager GROND at the 2.2 m telescope on La Silla, Chile. The circle denotes the *Swift*/XRT error box. Some of the local standards of Table 2 are labeled in the i' image; the remaining ones are outside the field shown here.

those of the exceptional bright GRBs 990123 and 080319B (Akerlof et al. 1999; Kann et al. 2007a; Racusin et al. 2008). To identify more "typical" afterglows at high redshift is a much more arduous task, requiring rapid response, multicolor observations, and ultimately rapid and deep spectroscopy. Such situations must inevitably be somewhat fortuitous, requiring a burst to be visible to large telescopes almost immediately after its occurrence, with good weather and appropriate instrumentation. This perhaps explains, at least in part, why bursts more distant than GRB 050904 have been extremely difficult to find. Yet, the present detection rate of GRBs at z 5 is about what is predicted on the basis of the star formation rate, so the lack of many high-z GRBs may well be due to the fact that there are few of them.

Here we report the discovery of GRB 080913 with *Swift* (Gehrels et al. 2004), and subsequent follow-up observations which identify this GRB to have originated at a redshift of $z = 6.7$, the highest known to date. In Section 2, we describe the observational effort in all wavelengths from hard X-rays to near-infrared, and present the results of these observations. In Section 3, we discuss several aspects of our observational findings.

2. OBSERVATIONS AND ANALYSIS RESULTS

2.1. Swift *BAT, XRT, and UVOT Measurements*

Swift/BAT triggered on GRB 080913 (trigger 324561) on 2008 September 13, at $T_0 = 06{:}46{:}54$ UT (Schady et al. 2008; Stamatikos et al. 2008). The BAT light curve shows multiple overlapping peaks with a T_{90} duration (the time interval during which 90% of the fluence is measured) of 8 ± 1 s. The peak count rate was 800 counts s^{-1} (15–350 keV). Using a 64 ms binned light curve, we compute spectral lags (e.g., Hakkila et al. 2007) of $0.114^{+0.098}_{-0.124}$ s for the 100–150 keV versus 50–100 keV band, and $0.148^{+0.094}_{-0.084}$ s for the 100–150 keV versus 15–50 keV band, consistent with an independent estimate by Xu (2008).

The time-averaged spectrum from $T_0 - 3.8$ s to $T_0 + 5.2$ s can be adequately fit by a power law with an exponential cutoff. This fit gives a photon index of 0.46 ± 0.70, and $E_{\rm peak} = 93 \pm 56$ keV (χ^2/dof $= 38.5/56$). The total fluence in the 15–150 keV band is $(5.6 \pm 0.6) \times 10^{-7}$ erg cm^{-2}, and the 1 s peak flux measured at $T_0 + 0.11$ s in the 15–150 keV band is 1.4 ± 0.2 ph cm^{-2} s^{-1}. A fit to a simple power law gives a photon index of 1.36 ± 0.15 (χ^2/dof $= 44.6/57$; all the quoted errors are at the 90% confidence level). A combined fit of the *Swift*/BAT (15–150 keV) and Konus-*Wind* (20–1300 keV) data (Pal'shin et al. 2008) in the time interval $T_0 - 4.1$ to $T_0 + 4.7$ s provides equally good fits for an expontentially cut-off power law (χ^2/dof $= 43.7/57$) or a Band function (χ^2/dof $= 43.9/57$). Using a Band function (Band et al. 1993; $\beta = -2.5$ fixed) yields $\alpha = -0.82^{+0.75}_{-0.53}$ and $E_{\rm peak} = 121^{+232}_{-39}$ keV (where $E_{\rm peak}$ is the energy at which most of the power is emitted, and α and β are the low- and high-energy photon indices, respectively), and an energy fluence in the 15–1000 keV band for the 8.8 s interval of 9×10^{-7} erg cm^{-2} (Pal'shin et al. 2008).

Swift slewed immediately to the burst and the X-ray Telescope (XRT; Burrows et al. 2005a) began its automated observing sequence at 06:48:30UT, 96 s after the trigger. A fading X-ray afterglow was detected; the UVOT-enhanced X-ray position (Beardmore et al. 2008) is R.A. (J2000.0) $= 04^{\rm h}22^{\rm m}54\overset{\rm s}{.}66$, decl. (J2000.0) $= -25^\circ 07' 46\overset{''}{.}2$, with an uncertainty of $1\overset{''}{.}9$ (radius, 90% confidence; see Figure 1).

The X-ray light curve (Figure 2) shows an initial decay rate ($F \propto t^{-\alpha}$) of $\alpha \sim 1.2$ from ~100 s to ~300 s and from ~400 to ~1100 s, with a likely small flare with the same decay slope afterward. At around T_0+1.8 ks ($\Delta T/T \sim 0.3$), there is a substantial flare with a factor of ~5 increase in count rate. The evolution thereafter is difficult to characterize due to the sparse coverage: it could be a continued decay from 2 ks to ~100 ks at the same slope of 1.2 but with an offset suggestive of energy injection, followed by a plateau, or it can be described as decaying at a slope of about 1.2 (Beardmore & Schady 2008) from 1200 s to 10^6 s with two flares superimposed.

The X-ray spectrum (using the *Swift* software package v2.9 and its associated set of calibration files) from T_0 + 108 s to 1920 s is well fit by an absorbed power law of photon index $\Gamma = 1.66 \pm 0.14$. A separate fit of the early flare and preflare times gives the same photon index (1.69 ± 0.25). The column density is consistent with the Galactic value of 3.2×10^{20}cm^{-2} in the direction of the burst (Kalberla et al.

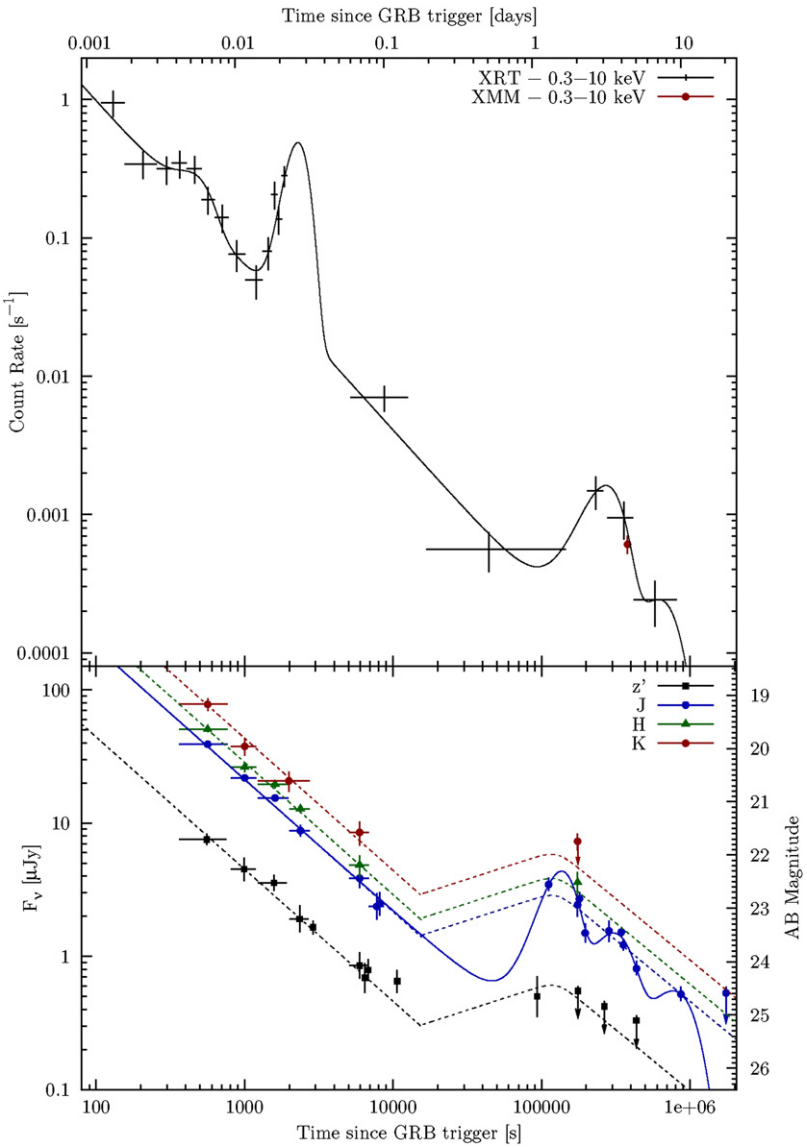

Figure 2. Optical/NIR (bottom) and X-ray light curve (top) of the GRB 080913 afterglow. The *XMM* data point has been converted to the *Swift*/XRT count rate axis using the best-fit spectral model. Several deviations from a canonical power law decay are apparent in both X-rays as well as optical. The early X-ray light curve ($T_0 + 200$ s until $T_0 + 2000$ s) is modeled by two log-Gaussian flares. For the optical light curve two different fits are shown: one for the plateau interpretation (dotted lines) and one for the flares interpretation (three log-Gaussians; solid line). The first model is motivated by the scenario of a plateau and late energy injection. In the second model, which assumes that X-ray flares are associated with optical flares, the last NIR data point is too bright, and consequently needs a third flare. The late Gemini upper limit supports this interpretation. The sum of the three log-Gaussian profiles roughly accounts for the flare at X-rays at the same time interval.

(A color version of this figure is available in the online journal.)

2005). The observed 0.3–10.0 keV flux at this time was $8.0^{+1.1}_{-1.0} \times 10^{-12}$erg cm^{-2}s^{-1}. This corresponds to an unabsorbed flux of $8.5^{+1.1}_{-1.0} \times 10^{-12}$erg cm^{-2}s^{-1} (0.3–10.0 keV).

UVOT observations in white light (100 s exposure) started 105 s after the BAT trigger, and subsequently all UVOT filters were used. The afterglow was not detected in any of the UVOT filters and the 3σ limiting white magnitude for the first finding chart exposure is >20.92; see Oates & Schady (2008) for the detailed upper limits in each filter.

2.2. Optical/NIR Photometry

2.2.1. Observations

GROND, a simultaneous seven-channel imager (Greiner et al. 2008a) mounted at the 2.2 m MPI/ESO telescope at La Silla (Chile), started observing the field at 06:52:57 UT, about 6 minutes after the GRB. The imaging sequence began with 66 s integrations in the $g'r'i'z'$ channels with gaps of about 16–18 s due to detector readout and preset to a new telescope dither position. After about 15 minutes, the exposure time was increased to 115 s, and after another 22 minutes to 375 s. In parallel, the three near-infrared channels JHK_S were operated with 10 s integrations, separated by 5 s due to readout, data-transfer, and K_S-band mirror dithering. At 09:46 UT, the start of nautical twilight (the Sun is 12° below the horizon), GROND switched to the "NIR-only" mode, in which the CCDs of the four visual channels are switched off, and only imaging in JHK_S is performed. Observations finally stopped completely at 10:07 UT. Further GROND imaging was performed on 2008 September 15, 07:12–09:28 UT, and 2008 September 16, 06:38–09:47 UT.

Table 1
Log of the Observations

Day/Time (UT in 2008)	Telescope/Instrument	Filter/ Grism	Exposure (s)	Brightness (mag)[a]
Sep 13 06:53–07:00	MPI/ESO 2.2m/GROND	$g'r'i'z'$	4×66	>23.3/>23.6/>23.0/21.71 ± 0.11
Sep 13 06:53–07:00	MPI/ESO 2.2m/GROND	JHK_S	24×10	19.96 ± 0.03/19.64 ± 0.05/19.17 ± 0.11
Sep 13 07:00–07:07	MPI/ESO 2.2m/GROND	$g'r'i'z'$	4×66	>23.3/>23.6/>22.9/22.27 ± 0.22
Sep 13 07:00–07:07	MPI/ESO 2.2m/GROND	JHK_S	24×10	20.59 ± 0.04/20.35 ± 0.08/19.96 ± 0.15
Sep 13 07:07–07:20	MPI/ESO 2.2m/GROND	$g'r'i'z'$	4×115	>23.8/>24.0/>23.5/22.52 ± 0.15
Sep 13 07:07–07:20	MPI/ESO 2.2m/GROND	JH	48×10	20.97 ± 0.04/20.68 ± 0.07
Sep 13 07:07–07:33	MPI/ESO 2.2m/GROND	K_S	96×10	20.61 ± 0.17
Sep 13 07:20–07:33	MPI/ESO 2.2m/GROND	$g'r'i'z'$	4×115	>23.6/>23.8/>23.3/23.20 ± 0.26
Sep 13 07:20–07:33	MPI/ESO 2.2m/GROND	JH	48×10	21.58 ± 0.11/21.14 ± 0.07
Sep 13 08:25–08:55	MPI/ESO 2.2m/GROND	$g'r'i'z'$	4×375	>24.4/>24.6/>24.1/24.54 ± 0.25
Sep 13 08:25–08:55	MPI/ESO 2.2m/GROND	JHK_S	120×10	22.47 ± 0.13/22.19 ± 0.17/21.58 ± 0.17
Sep 13 08:55–09:40	MPI/ESO 2.2m/GROND	$g'r'i'z'$	4×375 + 4×115	>24.5/>24.6/>24.2/>24.4
Sep 13 08:55–09:40	MPI/ESO 2.2m/GROND	JHK_S	120×10 + 48×10	23.00 ± 0.30/>22.40/>21.60
Sep 13 07:34–07:36	ESO VLT/FORS2	$z_{\rm Gunn}$	120	23.36 ± 0.13
Sep 13 07:37–07:39	ESO VLT/FORS2	I	80	>23.8
Sep 13 07:40–07:41	ESO VLT/FORS2	V	80	>24.0
Sep 13 07:42–07:44	ESO VLT/FORS2	B	150	>23.6
Sep 13 07:45–07:46	ESO VLT/FORS2	R	60	>24.1
Sep 13 08:34–08:36	ESO VLT/FORS2	$z_{\rm Gunn}$	120	24.31 ± 0.28
Sep 13 08:40–08:42	ESO VLT/FORS2	$z_{\rm Gunn}$	120	24.16 ± 0.20
Sep 13 08:52–09:22	ESO VLT/FORS2	grism 600z	1800	–
Sep 13 09:44–09:48	ESO VLT/FORS2	$z_{\rm Gunn}$	200	24.37 ± 0.21
Sep 13 09:52–10:02	ESO VLT/FORS2	grism 600z	600	–
Sep 13 09:02–09:12	ESO NTT/SOFI	J	10×60	23.18 ± 0.30
Sep 14 08:29–09:41	ESO VLT/FORS2	$z_{\rm Gunn}$	11×160	24.65 ± 0.37
Sep 14 12:49–15:02	Gemini-N/NIRI	J	53 × 60	22.59 ± 0.12
Sep 15 07:12–09:27	MPI/ESO 2.2m/GROND	$g'r'i'z'$	16×375	>24.8/>25.0/>24.3/>24.5
Sep 15 07:12–09:27	MPI/ESO 2.2m/GROND	JHK_S	480×10	22.97 ± 0.23/22.52 ± 0.20/>21.7
Sep 15 08:45–09:51	ESO NTT/SOFI	J	60×6×10	22.97 ± 0.16
Sep 15 12:55–14:36	Gemini-N/NIRI	J	74 × 60	23.50 ± 0.18
Sep 16 05:25–09:15	ESO VLT/FORS2	grism 600z	7×1800+900	–
Sep 16 06:38–09:46	MPI/ESO 2.2m/GROND	$g'r'i'z'$	24×375	>25.1/>25.3/>24.8/>25.0
Sep 16 06:38–09:46	MPI/ESO 2.2m/GROND	JHK_S	720×10	>23.2/>22.7/>22.0
Sep 16 12:40–14:49	Subaru/IRCS	J	54 × 120	23.46 ± 0.20
Sep 17 06:39–07:36	ESO VLT/HAWK-I	J	44×60	23.48 ± 0.09
Sep 17 08:51–09:48	ESO VLT/HAWK-I	J	44×60	23.72 ± 0.11
Sep 18 07:04–08.56	ESO VLT/FORS2	$z_{\rm Gunn}$	32×180	> 25.1
Sep 18 07:59–09:00	ESO VLT/HAWK-I	J	44×60	24.16 ± 0.13
Sep 23 07:03–09:52	ESO VLT/ISAAC	J	64×14×10	24.61 ± 0.13
Sep 29 07:19–08:03	ESO VLT/ISAAC	J	32×6×10	>23.4
Oct 03 12:56–15:28	Gemini-N/NIRI	J	116×60	>24.6

Note. [a] Not corrected for Galactic foreground reddening of $E(B-V) = 0.043$. Converted to the AB system for consistency with Figure 2, using the following coefficients for the J band: HAWK-I: +0.98 mag, Gemini-N: +0.96 mag, ISAAC: +0.96 mag, GROND: +0.91 mag, SOFI: +0.96 mag, Subaru: +0.94 mag.

Imaging was also secured immediately after the burst and on the subsequent nights at the VLT (ESO) with the Focal Reducer and Spectrograph FORS in filters *BVRIz*, and with ISAAC and HAWK-I in *J*. Further imaging was obtained with NTT/SOFI, Subaru/IRCS, and Gemini-N/NIRI in the *J* band (Table 1).

Data reduction was done in a standard way using IRAF routines. Photometric calibration of the GROND g', r', i', z' bands was performed using the Sloan spectrophotometric standard star SA95-142, which was observed shortly after the GRB 080913 field. Magnitudes are therefore given in AB magnitudes since this is the natural photometric system for GROND (see Greiner et al. 2008a). In order to match the different $z'J$-band filters used, the field calibration of the GROND filter magnitudes was compared against the VLT (or Gemini/Subaru) magnitudes using ∼50 field stars. For instance, the rms scatter between the GROND z' and FORS2 Gunn-z was < 0.06 mag, so no color transformations were applied. Calibration of the field in *JHK* was performed using Two Micron All Sky Survey (2MASS) stars which were chosen as close as possible to the GRB afterglow (and with a nicely sampled point-spread function), to reduce the error in the calibration due to flatfielding, which is (for GROND) 0.5%–1.0% on small scales and around 2% over the whole array. The magnitudes of the selected 2MASS stars were then transformed into the GROND filter system and finally into AB magnitudes using $J(\mathrm{AB}) = J(\mathrm{Vega}) + 0.91$, $H(\mathrm{AB}) = H(\mathrm{Vega}) + 1.38$, $K(\mathrm{AB}) = K(\mathrm{Vega}) + 1.81$ (for details, see Greiner et al. 2008a). In this way, a set of nine secondary standard stars was created (Table 2).

2.2.2. The Photometric Redshift Estimate

After stacking the GROND exposures taken during the first 16 minutes (06:53–07:07 UT), the GROND pipeline reduction (Küpcü Yoldaş et al. 2008) found a faint source at R.A. (J2000.0) = $04^{\rm h}22^{\rm m}54\overset{\rm s}{.}74$, decl. (J2000.0) = $-25^\circ07'46\overset{''}{.}2$ ($0\overset{''}{.}5$ error),

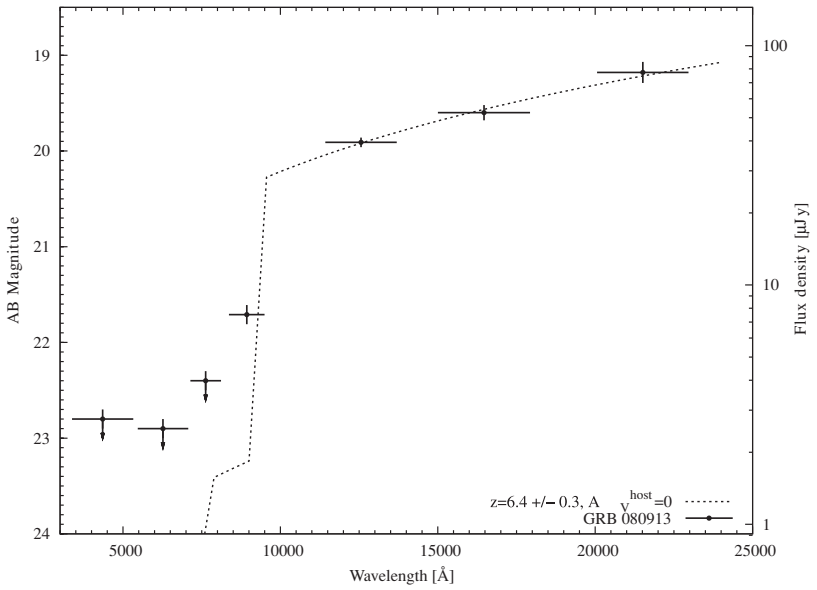

Figure 3. SED of the afterglow of GRB 080913, obtained about 10 minutes after the GRB. The drop-out shortward of the z' band is clearly visible. This information was used to trigger spectroscopy with VLT/FORS2 which then started with grism 600z, selected as compromise between spectral resolution and faintness of the afterglow, about 2 hr after the GRB. Shifting the latter VLT magnitudes in *BVRIz* to the earlier time of the GROND measurement, the upper limits would be $B > 22.5$, $V > 22.6$, $R > 22.5$, and $I > 22.0$, thus not more constraining than the GROND limits.

Table 2
Local Photometric Standards; the JHK_S Magnitudes are in the Vega System, the $g'r'i'z'$ Magnitudes in AB.

No	Coordinates (J2000)	g'	r'	i'	z'	J	H	K_S
1	$04^h22^m56\overset{s}{.}1$ –25°07′10″	–	20.52 ± 0.02	19.28 ± 0.01	18.72 ± 0.01	17.50 ± 0.04	16.90 ± 0.03	16.90 ± 0.06
2	$04^h22^m54\overset{s}{.}4$ –25°07′27″	–	–	–	–	20.26 ± 0.05	19.31 ± 0.06	18.61 ± 0.13
3	$04^h22^m53\overset{s}{.}9$ –25°07′37″	–	–	–	–	19.97 ± 0.05	18.91 ± 0.05	18.10 ± 0.11
4	$04^h22^m55\overset{s}{.}2$ –25°07′39″	16.97 ± 0.01	16.14 ± 0.01	15.82 ± 0.01	15.65 ± 0.01	14.76 ± 0.02	14.25 ± 0.03	14.20 ± 0.04
5	$04^h22^m55\overset{s}{.}3$ –25°07′49″	–	–	–	–	20.01 ± 0.05	18.86 ± 0.06	18.57 ± 0.14
6	$04^h22^m54\overset{s}{.}2$ –25°07′57″	15.96 ± 0.01	15.57 ± 0.01	15.39 ± 0.01	15.29 ± 0.01	14.54 ± 0.02	14.18 ± 0.03	14.19 ± 0.04
7	$04^h22^m55\overset{s}{.}8$ –25°08′04″	18.73 ± 0.01	17.26 ± 0.01	16.22 ± 0.01	15.76 ± 0.01	14.57 ± 0.02	13.88 ± 0.03	13.70 ± 0.05
8	$04^h22^m57\overset{s}{.}4$ –25°08′11″	–	20.90 ± 0.04	20.20 ± 0.03	19.81 ± 0.04	18.34 ± 0.05	17.43 ± 0.04	16.71 ± 0.07
9	$04^h22^m52\overset{s}{.}7$ –25°08′36″	–	20.04 ± 0.02	18.71 ± 0.01	18.15 ± 0.01	16.90 ± 0.04	16.24 ± 0.03	16.17 ± 0.05

which was only detected in the $z'JHK_S$ bands, but not in shorter-wavelength bands (Figures 1 and 3), and thus suggested a redshift above 6 (Rossi et al. 2008; Greiner et al. 2008b). This was confirmed by VLT/FORS2 *RzIVBR* imaging, starting 45 minutes after the burst, the only detection being in the z band with $z(\mathrm{AB}) = 23.1$ (Vreeswijk et al. 2008). A fit to the simultaneously obtained seven-filter GROND spectral energy distribution (SED) using Hyper-z (Bolzonella et al. 2000) results in a photometric redshift of $z = 6.44 \pm 0.30$ (Figure 3; Greiner et al. 2008b).

2.2.3. The Afterglow Light Curve

The optical/NIR light curve (Figure 2) during the first few hours is described by a power law of 0.98 ± 0.05. The third GROND data point at 2000 s postburst is simultaneous to the X-ray flare, and is clearly above that power-law decay, suggesting that we see enhanced optical emission from that X-ray flare (Figure 2). If we ignore this third data point, the reduced χ^2 improves substantially, and the new power law decay is 1.03 ± 0.02. After the GRB location became visible again after 2 days (clouds prevented observations on September 14), at ∼180 ks post burst, the optical/NIR brightness as measured by GROND is nearly identical to that at 10 ks, suggesting a prolonged plateau phase (Figure 2). Later monitoring with GROND, VLT, NTT, Gemini-N and Subaru shows pronounced variability which can be, in principle, fit by three log-Gaussian flares. At the same time, also the X-ray light curve shows an enhanced flux level. It is likely, though it cannot be proven, that the X-ray light curve also consisted of flares, which are not resolved due to the faintness and the somewhat poorer sampling as compared to the optical/NIR band. In any case, the enhanced X-ray flux lets us prefer that the optical lightcurve is probably a flare rather than a plateau. Our J-band data point ($J = 24.61 \pm 0.13$) at 8×10^5 s is again well above a power-law extrapolation after the two flares.

2.2.4. The GROND-derived Afterglow Broad-band Spectrum

We fit the NIR SED (the z' and Gunn-z bands are affected by Ly-α and are not included) with no extinction and with three different dust models (LMC, MW, SMC). Here we assume that the afterglow spectrum should have a power-law shape, with $F \propto \nu^{-\beta}$ (note that the spectral index β is related to the photon index Γ from the X-ray spectral fitting by $\beta = \Gamma - 1$). The best-fit power law has $\beta = 1.12 \pm 0.16$. No evidence for extinction in the host frame is found.

2.3. Optical Spectroscopy

Immediately after determining the photo-z, we triggered our target-of-opportunity program at ESO (PI: J. Greiner), and

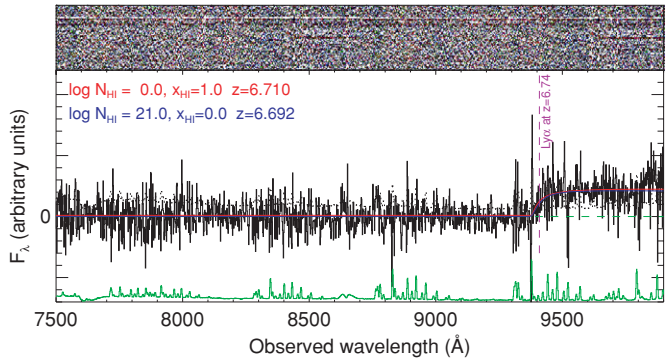

Figure 4. Optical spectrum of the afterglow of GRB 080913 obtained with VLT/FORS2. The spectrum shown corresponds to the 2400 s exposure on 2008 September 13. The break due to the Lyα forest is clearly visible at 9400 Å. The bottom green curve shows sky spectrum, and the dotted line superimposed on the spectrum shows the error spectrum (noise) after the sky subtraction. Two model fits are shown (see the text).

(A color version of this figure is available in the online journal.)

obtained an optical spectrum of the afterglow of GRB 080913 in the 7500–10500 Å (grism 600z) region with FORS2/VLT on 2008 September 13. Only one 1800 s and one 600 s exposure were possible before dawn. The spectrum revealed a continuum disappearing blueward of a break around 9400 Å. Interpreting this break as the onset of the Lyman-α forest a preliminary redshift estimate of $z = 6.7$ was inferred (Fynbo et al. 2008b). A second set of exposures (7×1800 s) was acquired on 2008 September 16, with identical settings. The first night's spectrum is shown in Figure 4. The afterglow is also detected in the spectrum from two nights later, but with a smaller signal-to-noise ratio (S/N).

In order to constrain the redshift we first tried to search the spectrum for a significant metal absorption line. Unfortunately, no such line seems to be present in the spectrum. Therefore, the redshift can be based on the shape of the break at 9400 Å only: the flux is zero in the interval 7500–9400 Å, and clearly nonzero above 9400 Å, strongly supporting the detection of the Lyman break, i.e., a high-z object. We first tried a simple cross-correlation analysis using the "fxcor" task in IRAF. As templates we used the spectra of GRBs 050730 (z =3.969) and 060206 (z =4.048, redward of the center of the DLAs of these spectra). This analysis leads to a redshift of $z = 6.69 \pm 0.02$.

In order to make a more refined analysis we follow Totani et al. (2006) and fit the spectrum using two different assumptions about the origin of the break. The damping wing can either be interpreted as that of a damped Lyman-α (DLA) absorber in the host galaxy (Jakobsson et al. 2006b) or that of IGM neutral hydrogen (Madau & Rees 2000). We performed a chi-square analysis with the three parameters of $N_{\rm H\,I}$ (column density of DLA), $x_{\rm H\,I}$ (neutral fraction of IGM hydrogen), and z (redshift of the GRB). We assume that the DLA has the same redshift z, and the neutral IGM hydrogen is distributed from $z_{{\rm IGM},l}$ to z, meaning that there is no ionized bubble around the host galaxy. We assume $z_{{\rm IGM},l} = 6.0$, but this has little influence on the fit if $z - z_{{\rm IGM},l} >\sim 0.3$ (Totani et al. 2006). No prior is assumed for these model parameters. We obtained the best fit at $(\log N_{\rm H\,I}/{\rm cm}^{-2}, x_{\rm H\,I}, z) = (19.74, 1.0, 6.71)$, in which the damping wing is dominated by IGM. On the other hand, a DLA dominating case of (21.41, 0.001, 6.68) is also consistent with the data (1.2σ deviation from the best fit). Marginalizing $N_{\rm H\,I}$ and $x_{\rm H\,I}$, we obtain the 95.4% confidence limits on z as $6.67 < z < 6.72$, where the DLA and IGM are dominant in the lower and upper limits, respectively.

When we fix $x_{\rm H\,I} = 0.001$ (almost fully ionized IGM with negligible effect on the damping wing), we obtain 95.4% limits on $N_{\rm H\,I}$ as $20.29 < \log N_{\rm H\,I}/{\rm cm}^{-2} < 21.41$ marginalizing the redshift, with the best-fit value of $\log N_{\rm H\,I}/{\rm cm}^{-2} = 20.99$ at $z = 6.69$. When we assume that $N_{\rm H\,I}$ is negligibly small, we obtain a 95.4% lower-limit of $x_{\rm H\,I} > 0.35$ again marginalizing redshift. This means that, if the column density of the DLA in the host galaxy is sufficiently small to have a negligible effect on the observed damping wing, we need a significantly neutral IGM indicating that the reionization has not yet been completed at $z = 6.7$. Although this possibility is completely dependent on the assumption about DLA column density, it is not in contradiction with the 95% upper bound of $x_{\rm H\,I} < 0.60$ at $z = 6.3$ obtained from GRB 050904 (Totani et al. 2006). A significantly high neutral fraction of IGM at $z \gtrsim 6.7$ has also been implied from evidence for the GP damping wing in the spectra of $z = 6$ quasars (Mesinger & Haiman 2004, 2007) and the luminosity function evolution of Ly-α emitters (Kobayashi et al. 2007; Ota et al. 2008). These claims remain controversial, since different sightlines to quasars can produce large variations in the Ly-α absorption spectra (Bolton & Haehnelt 2007), and the apparent evolution of the Ly-α luminosity function may be explained by the evolution of the mean IGM density alone (Dijkstra et al. 2007).

2.4. The X-ray to Optical SED

The combined XRT and GROND/VLT SED was fit (except the z' band since it is affected by Ly-α) in three separate time intervals: the early decay except the second flare at $T_0 + 2000$ s, i.e. the interval 360–1200 s, the intermediate brightness level (5.16–12.6 ks), and at very late times (16.7–550 ks). We used a single as well as a broken power law, modified by dust extinction in the rest-frame FUV (zdust in XSPEC) for Milky Way, SMC and LMC, and hydrogen absorption at X-rays. The hydrogen absorption was fit for all the data, and then fixed at that value for the individual intervals. For the single power-law fit, we obtain a photon index of 1.7 ± 0.1 and a marginal reddening $E(B-V)$ of 0.096 ± 0.045 (χ^2/dof = 8.4/10) assuming LMC dust in the GRB host (see Figure 5). The results for SMC or MW dust are the same within the errors. Forcing the dust extinction to be zero results in a somewhat worse fit (χ^2/dof = 15/11). Since the dust at high-z may have different properties than in the local universe, we also fitted the supernovae induced dust extinction curve (Maiolino et al. 2001; Stratta et al. 2007), which results in $A_{\rm V} = 0.07 \pm 0.11$ mag $\left(\chi^2_{\rm red} = 0.94\right)$. We note that the GROND-XRT SED for this first time interval likely is affected by enhanced X-ray emission from the early flare (at 300–700 s), thus resulting in a flatter spectral slope than derived from the GROND data alone.

Using a broken power-law fit instead and fixing the XRT power law slope to 1.7 (see above), we obtain a photon index of $2.1^{+0.45}_{-0.03}$ for the GROND data (corresponding to the energy index of 1.1; see above) and negligible dust, i.e. $E(B-V) = 0.026^{+0.027}_{-0.054}$. This implies that the early X-ray afterglow emission is contaminated by the flare emission, leading to a flatter X-ray-to-optical SED. The goodness of the fit is not better than the single power-law fit (χ^2/dof = 11/9), so a broken power law is anyway not required by the data. For the two late-time SEDs, the uncertainties are larger due to the lower S/N and thus are equally well fit by a single power law.

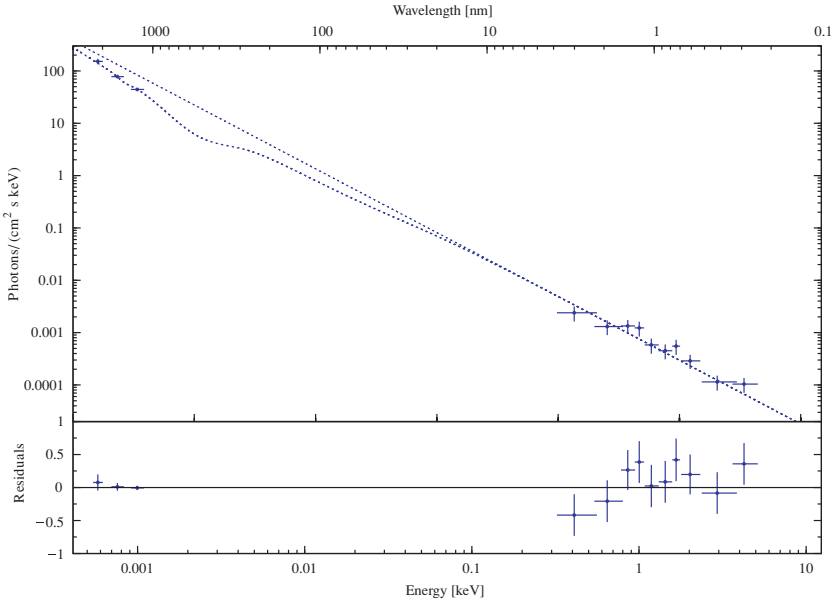

Figure 5. Combined *Swift*/XRT and GROND SED for the time interval 200–1800 s after the burst. Shown is the fit with a single power law (for parameters, see the text).

(A color version of this figure is available in the online journal.)

2.5. *Late-time* XMM-Newton *Observation*

A triggered *XMM-Newton* observation was performed at 380 ks postburst. The afterglow is clearly detected. There is no evidence for any variability in the *XMM* lightcurve. The spectrum is acceptably fit with a power law with fixed Galactic absorption (3.2×10^{20} cm^{-2}). The best-fit photon index is $\Gamma = 2.0 \pm 0.2$. The unabsorbed flux is 2.2×10^{-14} erg cm^{-2} s^{-1} in the 0.3–10.0 keV band.

3. DISCUSSION

With $z = 6.695 \pm 0.025$, GRB 080913 is the most distant burst detected so far (and actually the second most distant spectroscopically confirmed object after a galaxy at $z = 6.96$, as well as the most distant X-ray source) for which a redshift has been determined (Iye 2008). In a concordance cosmology model (Spergel et al. 2003), with $H_0 = 71$ km s^{-1} Mpc^{-1}, $\Omega_M = 0.27$, $\Omega_\Lambda = 0.73$, the corresponding luminosity distance is 67 Gpc (2×10^{29} cm), and the age of the universe at that time is 825 Myr (6% of the present age).

3.1. Comparison to Other GRBs

3.1.1. GRB Properties

With the above numbers, the isotropic energy release is $E_{\rm iso} \approx 7 \times 10^{52}$ erg (1 keV − 10 MeV; see also Pal'shin et al. 2008). This is typical of the long GRB population at large. Compared to the properties of GRB 050904, the other previous GRB at $z > 6$, GRB 080913 has a substantially shorter duration, lower gamma-ray luminosity as well as much dimmer (∼5 mag at early times) afterglow. Thus, it appears that gamma-ray bursts at this early epoch show the same large diversity as the low-z bursts.

3.1.2. On the Burst Duration

The observed bimodal hardness-duration distribution of the prompt emission from GRBs has led to the distinction between long- (>2 s) and short-duration (<2 s) bursts (Mazets et al. 1981; Norris et al. 1984; Kouveliotou et al. 1993). Long-duration gamma-ray bursts are thought to arise in jets created by the collapse of a massive star, short-duration bursts have been suggested to emerge from a compact binary merger (Eichler et al. 1989; Paczyński 1987; Woosley 1993). GRB 080913 is, in its rest frame, relatively short and hard, with a rest frame duration around 1 s, and rest frame $E_{\rm peak} \sim 990$ keV for a Band function fit (Pal'shin et al. 2008). Other moderately high redshift bursts with rest-frame duration shorter than 2 s are GRBs 060206 ($T_{90} = 7 \pm 2$ s, $z = 4.0$), 051016B ($T_{90} = 4 \pm 0.1$ s, $z = 0.94$), 050406 ($T_{90} = 5 \pm 1$ s, $z = 2.44$), 050416A ($T_{90} = 2.4 \pm 0.2$ s, $z = 0.6535$), 000301C ($T_{90} \sim 2$ s, $z = 2.03$), 040924 ($T_{90} \sim 1.5$ s, $z = 0.859$), and 050922C ($T_{90} = 5 \pm 1$ s, $z = 2.2$; Levan et al. 2007), as well as GRBs 060223 ($T_{90} = 11 \pm 2$ s, $z = 4.41$), 060926 ($T_{90} = 8.0 \pm 0.1$ s, $z = 3.20$), 070506 ($T_{90} = 4.3 \pm 0.3$ s, $z = 2.31$), 071020 ($T_{90} = 4.2 \pm 0.2$ s, $z = 2.145$), and 080520 ($T_{90} = 2.8 \pm 0.7$ s, $z = 1.545$). These bursts all show several of the typical signs of a massive stellar origin, e.g., star-forming host galaxies, a gas-rich line of sight, and (in the case of GRB 050416A) an associated supernova. Since the long- to short-duration separation at ∼2 s was derived in the observer's frame for BATSE bursts for which redshifts are not available in general, we consider it most plausible that GRB 080913, despite its intrinsically relatively short duration, is a member of the long-duration population of GRBs. Also, GRB 080913 is compatible with the previously known lag-luminosity correlation of long-duration bursts and is also consistent with the Amati relation Amati et al. (2002). While a merger origin for GRB 080913 cannot be definitely ruled out, the short duration also leads to an interesting question for the collapsar scenario: how can a massive star produce a burst as short as 1s?

3.1.3. Afterglow Properties

In order to compare the afterglow of GRB 080913 with those of previous GRBs we analyze its intrinsic properties both in the optical as well as the X-ray regime within large afterglow samples obtained for other GRBs. Using $\beta = 1.1$ we shift

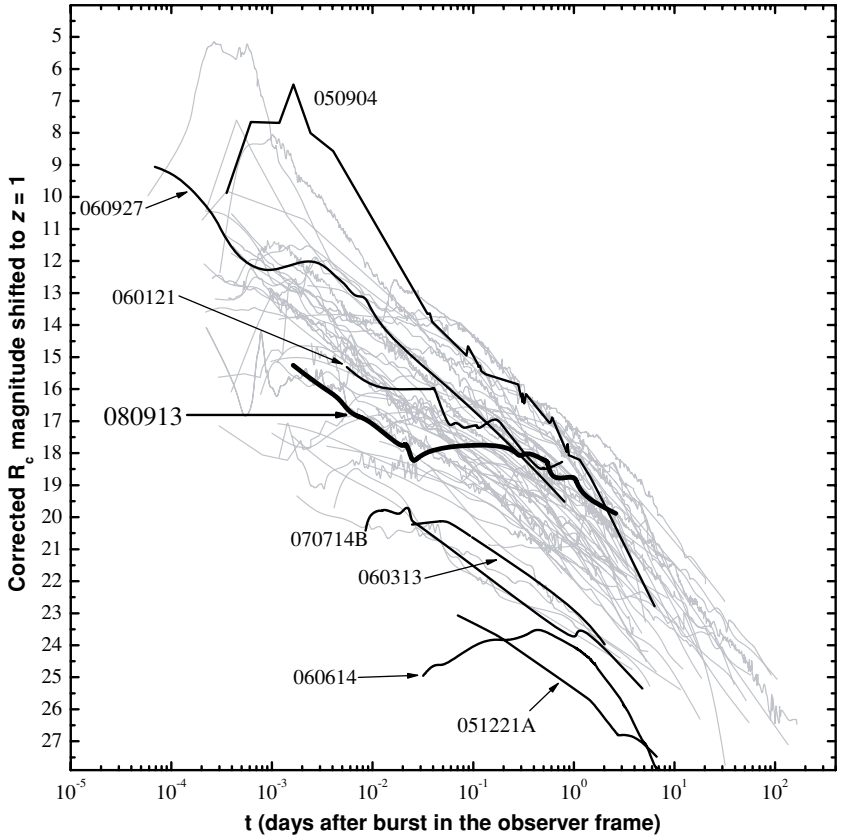

Figure 6. Optical/NIR afterglow of GRB 080913 (thick black line), shifted to the R_C band and to a redshift $z = 1$, and compared with other GRB afterglows, also at $z = 1$ (Kann et al. 2007b, 2008). At early times, the optical/NIR afterglow of GRB 080913 is fainter than the bulk of the long GRBs with detected afterglows, and at late times it is brighter. With the possible exception of GRB 060121 (if it lies at $z = 4.6$; De Ugarte Postigo et al. 2006), the optical/NIR afterglow of GRB 080913 is also much brighter than even those of bright short GRBs.

the light curve to $z = 1$ following Kann et al. (2006). The result is presented in Figure 6, and compared with other GRB afterglow light curves. At early times, the afterglow is fainter than the mean of the sample, and especially much fainter than the optical afterglows of the GRBs with the second and third highest redshifts, GRB 050904 and GRB 060927, respectively. At one day after the GRB at $z = 1$, following a strong rebrightening, $R_C = 18.80 \pm 0.13$ and $M_B = -24.1 \pm 0.2$, which is brighter than the mean of the sample of Kann et al. (2007b), $\overline{M_B} = -23.0 \pm 0.4$, but not exceedingly so. Indeed, even after the strong rebrightening, there are several afterglows that are considerably brighter at this time in the same frame.

Figure 7 shows the luminosity evolution of the X-ray afterglow of GRB 080913 in comparison to the population of 110 X-ray afterglows of *Swift* bursts with known redshift detected by July 2008. The original data were obtained from the X-ray light curve repository (Evans et al. 2007). Luminosities were calculated following Nousek et al. (2006). The spectral slope β of the SED was obtained by fitting an absorbed power law, $F(E_{\rm obs}) \sim \exp\left(-N_{\rm H}^{\rm Gal}\,\sigma(E_{\rm obs})\right)\exp\left(-N_{\rm H}^{\rm host}\,\sigma(E_{\rm host})\right)\nu^{-\beta}$ with $E_{\rm host} = E_{\rm obs}\,(1+z)$, while fixing the Galactic column density to the value given by Kalberla et al. (2005). In Figure 7 the low-luminosity end is mainly occupied by short burst afterglows, which on average separate clearly from their long burst cousins. Some short bursts are indicated (GRBs 051221A, 060313, 060121 at $z = 4.6$; De Ugarte Postigo et al. 2006, or GRB 070714B) as well as the second and third most distant bursts GRB 050904 (Haislip et al. 2006; Kawai et al. 2006) and GRB 060927 (Ruiz-Velasco et al. 2007). These events, together

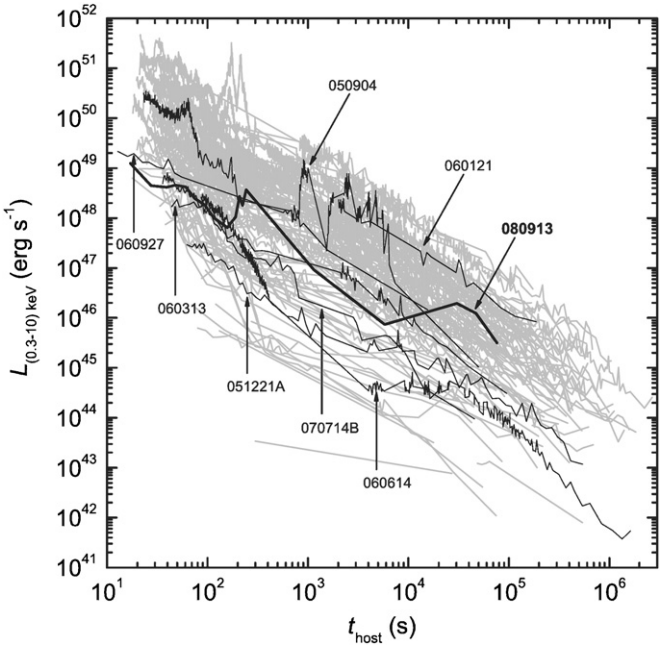

Figure 7. X-ray afterglow of GRB 080913 in comparison with 110 X-ray afterglows with known redshift discovered by *Swift* since 2005.

with GRB 080913, indicate a rather broad luminosity distribution even at high redshift. Figure 7 makes it clear that similar to the optical/NIR bands, the rest-frame X-ray afterglow of GRB

080913 is rather faint. Compared to the long-burst ensemble, it belongs to the low-luminosity members, while compared to the short-burst ensemble it occupies the high-luminosity region.

3.2. Modelling of the Afterglow

The temporal and spectral power law indices of the early ($t < t_{b1} \sim 10^4$ s) optical/NIR afterglow, $\alpha_{\rm opt,1} = 1.03 \pm 0.02$ and $\beta_{\rm opt} = 1.12 \pm 0.16$, are consistent with the closure relation $\alpha_{\rm opt,1} - 1.5\beta_{\rm opt} \sim -0.5$, which corresponds to the standard model with the optical band above the cooling frequency ν_c and the typical synchrotron frequency ν_m. The electron energy distribution index $p \sim 2.2$, inferred from $p = (4\alpha_{\rm opt,1} + 2)/3$ and/or $p = 2\beta_{\rm opt}$ of the standard model prediction (Mészáros & Rees 1997; Sari et al. 1998), is identical to the canonical one.

The early optical/NIR data can also constrain the values of other parameters (e.g., initial isotropic kinetic energy E_i, energy fraction in electrons ϵ_e and that in magnetic fields ϵ_B) of the forward shock model. If the circumburst environment is interstellar medium (ISM), the requirement of $\nu_{\rm opt} > \max(\nu_m, \nu_c)$ at $t = 560$ s and the H-band flux density $F_{\nu_H} \sim 4\mu$Jy at $t = t_{b1}$ can be translated to a set of loose constraints. In general, $10^{-5} < \epsilon_B < \epsilon_e < 1$, $E_{i,53} \leqslant 1.0$ and/or a density of $n \geqslant 100$ cm^{-3} can fit the afterglow, which is quite reasonable except maybe for the relatively high density. If the circumburst environment is a free wind, then the same observational constraints would require a more ad hoc set of parameters, i.e., $10^{-5} < \epsilon_B < \epsilon_e < 1$, $E_{i,53} \leqslant 1.0$ and $A_* \geqslant 1.0$ (where $A_* = A/(5 \times 10^{11}\,{\rm g\,cm^{-1}})$, and A is the normalization in the density profile $\rho = Ar^{-2}$). While a high-density medium is expected at high z (e.g., Gou et al. 2007), a large wind parameter $A_* \geqslant 1.0$ is not expected in view of the low stellar metallicity at high z. We therefore conclude that the afterglow modeling favors a constant density medium, although a stellar wind medium is not ruled out.

After the early decay, the afterglow intensity enters a plateau/flares phase. Due to the lower S/N the optical to X-ray SED with a photon index of 1.94 ± 0.20 now has larger error bars, but is still consistent with $\beta_{OX} \sim 1.0$ which indicates that the emission of both bands possibly has the same origin.

For the flares interpretation (see the solid line in Figure 2), the late time optical/NIR light curve is fit with log-Gaussian functions superimposed to the initial unbroken power law decay with temporal index fixed to be $\alpha_{\rm opt,1} = 1.03$. The best-fit amplitude and midtime of the optical flares are $F_{\nu_J,p} = 2.9 \pm 1.2\,\mu$Jy, $t_p = (1.33 \pm 0.17) \times 10^5$ s for the first flare, $F_{\nu_J,p} = (0.95 \pm 0.28)\,\mu$Jy, $t_p = (3.00 \pm 0.43) \times 10^5$ s for the second flare, and $F_{\nu_J,p} = (0.52 \pm 0.05)\,\mu$Jy, $t_p = (7.7 \pm 0.4) \times 10^5$ s for the third flare. The late time X-ray flare happens almost simultaneously with the optical flares. These late flares together with the early two X-ray flares (at T_0 + 300 s and T_0 + 2000 s) are very likely the emission from late internal shocks, as already detected in many previous *Swift* GRBs, long or short, and in GRB 050904 at comparable redshift (Burrows et al. 2005b; Barthelmy et al. 2005; Watson et al. 2006; Cusumano et al. 2006). The central engine of GRB 080913 in this case has accelerated and emitted relativistic ejecta intermittently for a whole period of at least $\sim 4 \times 10^4$ s in its rest frame.

For the plateau interpretation (see the dotted lines of Figure 2), the late time optical light curve can be fit by a broken power law with $\alpha_{\rm opt,2} = -0.19^{+0.15}_{-0.16}$ during the plateau until $t = t_{b2} = 1.16^{+0.19}_{-0.17} \times 10^5$ s, and $\alpha_3 = 0.92^{+0.09}_{-0.08}$ after the plateau. A joint fit combining the optical data with the X-ray data does not change the above values significantly, though the rising in X-rays between $T_0 + 50$ ks and $T_0 + 200$ ks is more pronounced than at optical/NIR wavelengths. The nearly achromatic beginning and ending times of the plateau, no significant spectral evolution across the break, and nearly same decay rate before and after the plateau (if averaging over the short-scale variability) all suggest that the rebrightening is due to the forward shock emission with a continuous energy injection, either due to a long-term central engine injecting energy in the form of Poynting flux (Dai & Lu 1998; Zhang & Mészáros 2002) or due to spread of the ejecta Lorentz factor distribution (Rees & Mészáros 1998; Sari & Mészáros 2000; Zhang & Mészáros 2002). In the former model, the Poynting flux luminosity from a spinning down central magnetar or black hole is $L = L_0(1+t/T_0)^{-2}$, while in the latter model the mass–Lorentz factor distribution may be modeled as $M(>\Gamma) \propto \Gamma^{-s}$. The total energy in the forward shock during the plateau phase increases with time as t^a. Using the optical spectral index, we can derive $a = 2\Delta\alpha_{\rm opt}/(1 + \beta_{\rm opt}) = 1.15 \pm 0.16$, where $\Delta\alpha_{\rm opt} = \alpha_{\rm opt,1} - \alpha_{\rm opt,2} = 1.22 \pm 0.15$. Therefore, the total energy has increased by a factor of $(t_{b2}/t_{b1})^a \sim 12$ compared to its initial value E_i. According to Table 2 of Zhang et al. (2006), we obtain $q = 1 - a = -0.15 \pm 0.16$, $s = (7a + 3)/(3 - a) = 6.0 \pm 0.8$ (ISM) and $s = (3a + 1)/(1 - a) = -29.7 \pm 31.8$ (wind). The value $q \sim 0$ is quite consistent with the Poynting flux injection model for times earlier than the central engine spin down time scale ($t < T_0$).

3.3. On High-Redshift Indicators

Various redshift indicators have been proposed in the past with the aim of selecting, based on high-energy data, candidates for high-redshift GRBs. Those include *Swift*/BAT properties such as burst duration ($T_{90} > 60$ s), peak photon flux (< 1 ph s^{-1} cm^{-2}), and spectral steepness (Campana et al. 2007; Salvaterra et al. 2007; Ukwatta et al. 2008), slowly rising GRB profiles (BAT image triggers as opposed to rate triggers), or the "pseudo"-redshift (in this case $z = 2.5$–6.0) based on the peak energy (Pelangeon 2006). For GRB 080913, most of these indicators have failed (in fact also for GRB 060927 at $z = 5.47$), except for the excess-$N_{\rm H}$ method (Grupe et al. 2007). As these criteria are statistical in nature, outliers are possible. However, the parameters of this burst demonstrate that one should not bias the search for high-z events on those criteria. High-z GRBs are so rare that we cannot afford to loose the rare events that do occur. The trigger criteria we are setting up for our follow-up observations should rather include false triggers than exclude the true ones. The only secure way to find these high-z events is by simultaneous optical/NIR follow-up observations to establish their drop-out nature from the colors of the afterglows.

3.4. GRBs at $z > 6$

GRB 080913 is a proof that GRBs do occur at $z \gtrsim 6.7$ and hence that a mechanism for star formation and evolution leading to a burst of this duration was in place at this time. As we move to higher and higher redshifts the fraction of massive stars that are of population III (low metallicity) will increase. When this happens is strongly dependent on the strength of winds from the first stars and the efficiency of mixing of the metals (Scannapieco et al. 2006). In most models population III stars and stars only enriched by population III stars can be found down to $z \gtrsim 5$. Simulations of supernovae from population III stars suggest that the exploding stars will have hydrogen- and helium-rich outer

Table 3
Gamma-ray Bursts at $z > 5$.

GRB	Redshift	Reference
060522	5.11 ± 0.01	Cenko et al. (2006)
050814	5.77 ± 0.12	Jakobsson et al. (2006a); Curran et al. (2008)
060927	5.467	Ruiz-Velasco et al. (2007)
050904	6.295 ± 0.002	Kawai et al. (2006)
080913	6.695 ± 0.025	This work

layers (Ohkubo et al. 2006; Lawlor et al. 2007) and hence that they probably will not make GRBs at least by the collapsar mechanism. Concerning GRBs from binary population III stars it is debated how efficient they are in producing GRBs (Bromm & Loeb 2006; Belczynski et al. 2007).

Detecting high-redshift GRBs with *Swift* and measuring their redshifts with ground-based spectroscopy is of substantial interest because of the link between long-duration GRBs and the star formation rate density (SFRD). Indeed, the properties of GRB hosts and the distribution of GRB metallicities are consistent with the assumption that GRBs trace the bulk of the star-formation at $z \gtrsim 3$ (Jakobsson et al. 2005; Fynbo et al. 2008a). The existence of now five GRBs at $z > 5$ (Table 3), among them two at $z > 6$, out of a total of ∼150 GRBs with redshift estimates suggests that the global SFRD at $z > 5$ declines slowly and has a substantial value. Empirical calibrations of the GRB rate to the SFR at different redshifts have been attempted, and suggest that the high-z SFR must be high to accommodate the several observed high-z GRBs (Chary et al. 2007; Yüksel et al. 2008). Our detection of a GRB at $z = 6.7$ strengthens this result. This is also similar to the SFRD in the model assumed by Bromm & Loeb (2006) that predicts ∼ 10% of the *Swift* GRBs are at $z > 5$.

The discovery of bursts like GRB 080913 also allows us to study, in an unbiased way, some of the main questions in the evolution of the universe: where did most of the star formation happen at $z > 6$, and what was the nature of the sources responsible for the reionization? There is evidence that the bright $z > 6$ galaxies discovered using color–color (drop-out) selection or more advanced photometric redshifts are too rare to provide the total star formation rate as well as to *have done* the reionization (e.g., Bouwens et al. 2007). GRB measurements provide the tool to find the more typical galaxies responsible for the bulk of the production of ionizing photons (Ruiz-Velasco et al. 2007), and will allow further study of these galaxies in the future (e.g., with JWST or the ∼30 m ground-based telescopes).

The reionization history of the universe is currently not well constrained by observations. The *WMAP* data (Spergel et al. 2007) and the SDSS quasar data (Fan et al. 2006), and the GRB 050904 constraint (Totani et al. 2006) can accommodate several distinct reionization scenarios (e.g., Holder et al. 2003). In order to identify the correct scenario, bright beacons in the dark era (e.g., $z = 7$–1100) are needed. The discovery of GRB 080913 above the highest z for QSOs (CFHQS J2329-0301 at $z = 6.427 \pm 0.002$; Willot et al. 2007) re-enforced the possibility of using high-z GRBs to uncover the cosmic reionization history. The detection of lensed star formation at $z > 7$ (e.g., Bouwens et al. 2008) suggests that star formation in fact took place as early as $z \sim 8$–10 (at $t < 0.63$ Gyr). With hints for the first stars having formed as early as $20 \lesssim z \lesssim 60$ (Kogut et al. 2003; Bromm & Loeb 2006; Naoz & Bromberg 2007), GRBs are believed to exist as early as $z \sim 15$–20, and their gamma-ray and IR emissions are bright enough to be detected by the current instruments (Lamb & Reichart 2000; Ciardi & Loeb 2000; Gou et al. 2004). A caveat has been that the GRB host DLAs may have a large column density that would bury the signature of IGM absorption, as in the case of GRB 050904 (Totani et al. 2006). Cosmological SPH simulations (Nagamine et al. 2008), on the other hand, suggest that the GRB host DLA columns should degrade at high z, a prediction dictated by the fundamental structure formation theory. The low N(H I) associated with GRB 080913 (5×10^{20}cm^{-2} for the best-fit value and 1.4×10^{21}cm^{-2} for the maximum value) is generally consistent with such a prediction, though the medium N(H I) for $z > 4$ GRBs ($10^{21.45}$ cm^{-2}) is consistent with the medium value ($10^{21.3}$ cm^{-2}) for the total GRB population ($2 < z < 6.3$). In any case, high-z GRBs offer the promising possibility of probing cosmic reionization. Brighter GRBs at higher z's with a negligible N(H I) would allow mapping the IGM ionization fraction as a function of z in the dark era, and hence, greatly constrain the possible scenarios of cosmic reionization.

4. CONCLUSIONS

We have presented the observations that led to the discovery of GRB 080913 and the recognition of it being at redshift 6.7, the most distant GRB so far. This discovery was possible, first of all, due to the excellent properties of the *Swift* mission with its high sensitivity for GRBs and excellent localization capabilities based on the X-ray afterglows alone. Furthermore, this study demonstrates that 2 m class telescopes are sufficient to properly identify and determine reliable photometric redshifts of the most distant GRB afterglows. Here it is noteworthy that the afterglow of GRB 080913 was several magnitudes fainter than that of GRB 050904, the only other $z > 6$ GRB discovered so far. Hence, we can probe a significant fraction of the luminosity function of afterglows at these redshifts with 2 m class telescopes. We also note that many previously proposed high-z "indicators" primarily based on properties of the prompt emission have failed for GRB 080913, leaving photo-z determinations the only reliable method available.

While the afterglow of this GRB was particularly faint, we note that metallicity measurements as well as the determination of the neutral hydrogen fraction should be possible in general (as for GRB 050904), though likely not in all, cases. It is important to recognize, however, that studying the neutral hydrogen fraction in the highest redshift quasars is hopeless, and for galaxies complicated by their faintness and more structured continuum shape (McQuinn et al. 2008). Planned instrumentation in the near future with higher efficiency and higher spectral resolution such as X-shooter (Kaper et al. 2008) will help substantially in exploiting the promise that GRBs have as probes of the reionization epoch.

We are very grateful for the excellent support by the La Silla and Paranal Observatory staff, in particular to Stephane Brillant, Michelle Doherty, Carla Gil, Rachel Gilmour, Swetlana Hubrig, Heidi Korhonen, Chris Lidman, Emanuela Pompei, Julia Scharwächter, and Linda Schmidtobreick. We acknowledge discussions with J.P. Norris, T. Sakamoto, D. Grupe, E. Rol, N. Masetti, and E. Palazzi. We also acknowledge the support of the *XMM-Newton* SOC and the Project Scientist in scheduling and executing the target-of-opportunity observation. We thank the referee for useful comments, and G. Stratta for providing the SN extinction model template. T.K. acknowledges support by the DFG cluster of excellence 'Origin and Structure of the Universe', A.P.B. from STFC, and P.M.V. from the

EU under a Marie Curie Intra-European Fellowship, contract MEIF-CT-2006-041363. Part of the funding for GROND (both hardware as well as personnel) was generously granted from the Leibniz-Prize (DFG grant HA 1850/28-1) to Professor G. Hasinger (MPE). This work is partly based on observations collected at the European Southern Observatory, Chile under ESO proposal Nos. 081.A-0135, 081.A-0856 and 081.A-0966. The Dark Cosmology Centre is funded by the DNRF.

Facilities: Max Planck: 2.2m (GROND), VLT: Antu (FORS2), *Swift*, *XMM-Newton*

REFERENCES

Akerlof, C. W., et al. 1999, Nature, 398, 400
Amati, L., et al. 2002, A&A, 390, 81
Band, D., et al. 1993, ApJ, 413, 281
Barthelmy, S. D., et al. 2005, Nature, 438, 994
Beardmore, A. P., Evans, P. A., Goad, M. R., & Osborne, J. P. 2008, GCN Circ. 8219
Beardmore, A. P., & Schady, P. 2008, GCN Circ. 8226
Belczynski, K., Bulik, T., Heger, A., & Fryer, C. 2007, ApJ, 664, 986
Berger, E., et al. 2006, ApJ, 642, 979
Bolzonella, M., Miralles, J.-M., & Pelló, R. 2000, A&A, 363, 476
Bouwens, R. J., Illingworth, G. D., Franx, M., & Ford, H. 2007, ApJ, 670, 928
Bouwens, R. J., et al. 2008, ApJ, 678, 647
Bromm, V., & Loeb, A. 2006, ApJ, 642, 382
Bolton, J. S., & Haehnelt, M. G. 2007, MNRAS, 374, 493
Burrows, D. N., et al. 2005a, Space Sci. Rev., 120, 165
Burrows, D. N., et al. 2005b, Science, 309, 1833
Campana, S., Tagliaferri, G., & Malesani, D. 2007, A&A, 464, L25
Cenko, S. B., et al. 2006, GCN Circ. 5155
Chary, R., Berger, E., & Cowie, L. 2007, ApJ, 671, 272
Ciardi, B., & Loeb, A. 2000, ApJ, 540, 687
Curran, P. A., et al. 2008, A&A, 490, 1047
Cusumano, G., et al. 2006, Nature, 440, 164
Dai, Z. G., & Lu, T. 1998, A&A, 333, L87
De Ugarte Postigo, A., et al. 2006, ApJ, 648, L83
Dijkstra, M., Wyither, J. S. B., & Haiman, Z. 2007, MNRAS, 379, 253
Eichler, D, Livio, M., Piran, T., & Schramm, D. 1989, Nature, 340, 125
Evans, P. A., et al. 2007, A&A, 469, 379
Fan, X., Carilli, C. L., & Keating, B. 2006, ARA&A, 44, 415
Fynbo, J. P. U., et al. 2006, A&A, 451, L47
Fynbo, J. P. U., et al. 2008a, ApJ, 682, 321
Fynbo, J. P. U., et al. 2008b, GCN Circ. 8225
Galama, T. J., et al. 1998, Nature, 395, 670
Gehrels, N., et al. 2004, ApJ, 611, 1005
Gou, L. J., Fox, D. B., & Mészáros, P. 2007, ApJ, 668, 1083
Gou, L. J., et al. 2004, ApJ, 604, 508
Greiner, J., et al. 2008a, PASP, 120, 405
Greiner, J., Krühler, T., & Rossi, A. 2008b, GCN Circ. 8223
Grupe, D., et al. 2007, AJ, 133, 2216
Haislip, J. B., et al. 2006, Nature, 440, 181
Hakkila, J., et al. 2007, ApJS, 169, 62
Hartmann, D. H., et al. 2004, New Astron. Rev., 48, 237
Hjorth, J., et al. 2003, Nature, 423, 847
Holder, G. P., et al. 2003, ApJ, 595, 13
Iye, M. 2008, Proc. SPIE, 7016, 701602, in press (arXiv:0809.0050)
Jakobsson, P., et al. 2005, MNRAS, 362, 245
Jakobsson, P., et al. 2006a, A&A, 447, 897
Jakobsson, P., et al. 2006b, A&A, 460, L13
Kalberla, P. M. W., et al. 2005, A&A, 440, 775
Kann, D. A., Klose, S., & Zeh, A. 2006, ApJ, 641, 993
Kann, D. A., Masetti, N., & Klose, S. 2007a, AJ, 133, 1187
Kann, D. A., et al. 2007b, ApJ, submitted (arXiv:0712.2186)
Kann, D. A., et al. 2008, ApJ, submitted (arXiv:0804.1959)
Kaper, L., et al. 2008, Proc. ESO Workshop, Science with the VLT in the E-ELT era, ed. A. Moorwood (Berlin: Springer) (arXiv:0803.0609)
Kawai, N., et al. 2006, Nature, 440, 184
Kobayashi, M. A. R., Totani, T., & Nagashima, M. 2007, ApJ, 670, 919
Kogut, A., et al. 2003, ApJS, 148, 161
Kouveliotou, C., et al. 1993, ApJ, 413, L101
Küpcü Yoldaş, A., et al. 2008, in Gamma-Ray Bursts 2007, Proc. of the Santa Fe Conf., Oct. 2007, AIP Conf. Proc., 1000, 227
Lamb, D. Q., & Reichart, D. E. 2000, ApJ, 536, 1
Lawlor, T. M., Young, T. R., Johnson, T. A., & MacDonald, J. 2007, MNRAS, 384, 1533
Levan, A. J., et al. 2007, MNRAS, 378, 1439
Madau, P., & Rees, M. J. 2000, ApJ, 542, L69
Maiolino, R., et al. 2001, A&A, 365, 37
Mazets, E. P., et al. 1981, Ap&SS, 80, 3
McQuinn, M., et al. 2008, MNRAS, 388, 1101
Mesinger, A., & Haiman, Z. 2004, ApJ, 611, L69
Mesinger, A., & Haiman, Z. 2007, ApJ, 660, 923
Mészáros, P., & Rees, M. 1997, ApJ, 476, 232
Miralda Escude, J. 1998, ApJ, 501, 15
Nagamine, K., Zhang, B., & Hernquist, L. 2008, ApJ, 686, L57
Naoz, S., & Bromberg, O. 2007, MNRAS, 380, 757
Norris, J. P., Cline, T. L., Desai, U. D., & Teegarden, B. J. 1984, Nature, 308, 434
Nousek, R., et al. 2006, ApJ, 642, 389
Oates, S. R., & Schady, P. 2008, GCN Circ. 8224
Ohkubo, T., et al. 2006, ApJ, 645, 1352
Ota, K., et al. 2008, ApJ, 677, 12
Paczyński, B. 1987, ApJ, 317, L51
Pal'shin, V., et al. 2008, GCN Circ. 8256
Pelangeon, A. 2006, in AIP Conf. Proc. 836, Gamma-Ray Bursts in the Swift Era, ed. S. S. HoltGehrels & J. A. Nousek (New York: AIP), 149
Prochaska, X., Chen, H.-W., Dessauges-Zavadskyand, M., & Bloom, J. S. 2007, ApJ, 666, 267
Racusin, J. L., et al. 2008, Nature, 455, 183
Rees, M. J., & Mészáros, P. 1998, ApJ, 496, L1
Rossi, A., et al. 2008, GCN Circ. 8218
Ruiz-Velasco, A. E., et al. 2007, ApJ, 669, 1
Salvaterra, R., Campana, S., Chincarini, G., Tagliaferri, G., & Covino, S. 2007, MNRAS, 380, L45
Sari, R., & Mészáros, P. 2000, ApJ, 535, L33
Sari, R., Piran, T., & Narayan, R. 1998, ApJ, 497, L17
Savaglio, S. 2006, New J. Phys., 8, 195
Scannapieco, E., et al. 2006, ApJ, 653, 285
Schady, P., et al. 2008, GCN Circ. 8217
Spergel, D. N., et al. 2003, ApJS, 148, 175
Spergel, D. N., et al. 2007, ApJS, 170, 377
Stamatikos, M., et al. 2008, GCN Circ. 8222
Stanek, K. Z., et al. 2003, ApJ, 591, L17
Stratta, G., Maiolino, R., Fiore, F., & D'Elia, V. 2007, ApJ, 661, L9
Tagliaferri, G., et al. 2005, A&A, 443, L1
Totani, T. 1997, ApJ, 486, L71
Totani, T., et al. 2006, PASJ, 58, 485
Ukwatta, T. N., et al. 2008, in Gamma-Ray Bursts, Proc. of the Santa Fe Conf., Oct. 2007, AIP Conf. Proc., 1000, 166
Vreeswijk, P. M., et al. 2008, GCN Circ. 8221
Watson, D. J., et al. 2006, ApJ, 637, L69
Wijers, R. A. M. J., et al. 1998, MNRAS, 294, L13
Willot, C. J., et al. 2007, AJ, 134, 2435
Woosley, S. E. 1993, ApJ, 405, 273
Xu, D. 2008, GCN Circ. 8267
Yüksel, H., Kistler, M. D., Beacom, J. F., & Hopkins, A. M. 2008, ApJ, 683, L5
Zhang, B., & Mészáros, P. 2002, ApJ, 566, 712
Zhang, B., et al. 2006, ApJ, 642, 354